



# Micropatterning of the Ferroelectric Phase in a Poly(vinylidene difluoride) Film by Plasmonic Heating with Gold Nanocages

Jianhua Li, Miaoxin Yang, Xiaojun Sun, Xuan Yang, JiaJia Xue, Chunlei Zhu, Hong Liu, and Younan Xia\*

**Abstract:** Polymer thin films with patterned ferroelectric domains are attractive for a broad range of applications, including the fabrication of tactile sensors, infrared detectors, and non-volatile memories. Herein, we report the use of gold nanocages (AuNCs) as plasmonic nanostructures to induce a ferroelectric–paraelectric phase transition in a poly(vinylidene fluoride) (PVDF) thin film by leveraging its photothermal effect. This technique allows us to generate patterned domains of ferroelectric PVDF within just a few seconds. The incorporation of AuNCs significantly enhances the pyroelectric response of the ferroelectric film under near-infrared irradiation. We also demonstrate the use of such patterned ferroelectric films for near-infrared sensing/imaging.

**P**hotothermal conversion based on plasmonic nanostructures has been explored to induce localized heating of the host medium, which is highly attractive for a broad range of applications, including biomedicine,<sup>[1]</sup> steam generation,<sup>[2]</sup> optofluidics,<sup>[3]</sup> and acceleration of chemical reactions.<sup>[4]</sup> The heat transfer from a plasmonic nanoparticle to the host medium starts with the absorption of photons by localized surface plasmon resonance (LSPR) and the conversion of part of the photon energy into heat, which is then transferred to the surrounding medium.<sup>[5]</sup> Previous studies have demonstrated the use of such plasmonic heating to induce phase transitions in water,<sup>[2b]</sup> thermoresponsive copolymers,<sup>[6]</sup> and phase-changing materials.<sup>[7]</sup> These plasmon-assisted phase transitions in the host media can lead to various interesting physical changes in material properties, offering a powerful

approach to design and fabricate functional devices for an array of applications.

Ferroelectric polymers have attracted much interest as the next-generation piezo/pyroelectric materials owing to their feasibility in terms of solution processing, flexibility, low cost, and non-toxicity. Poly(vinylidene fluoride) (PVDF), one of the most commonly used ferroelectric polymers, possesses  $\alpha$ ,  $\beta$ , and  $\gamma$  phases.<sup>[8]</sup> Its piezo/pyroelectric properties have enabled the fabrication of film-based tactile sensors, infrared detectors, energy-harvesting devices, and non-volatile memories. To realize these applications, it is critical to pattern the ferroelectric phase (either  $\beta$  or  $\gamma$ ) rather than the paraelectric  $\alpha$  phase. Thus far, such patterning has mainly been achieved by irradiation etching<sup>[9]</sup> and imprinting lithography.<sup>[10]</sup> The former method may deteriorate the ferroelectric properties whereas it is not easy to obtain a freestanding and smooth polymer film using imprinting lithography without requiring multiple steps. PVDF generally exhibits a phase transition from the ferroelectric to the paraelectric phase when heated to temperatures near its melting point or the ferroelectric Curie temperature (ca. 170 °C).<sup>[11]</sup> As an alternative approach, Wegener et al. reported the patterning of a PVDF film by scanning a focused laser beam across the top aluminum electrode.<sup>[12]</sup> This method successfully generated depolarized stripes with a width of 80–90  $\mu\text{m}$  in a PVDF film, but the efficiency is expected to be relatively low owing to the high reflectance of the metal electrode and the one-direction heat transfer from the electrode to the film.

Herein, we demonstrate the use of plasmonic nanostructures to harvest photon energy as an effective means to induce ferroelectric–paraelectric phase transitions in a ferroelectric polymer film. Specifically, we mixed AuNCs with PVDF and then cast the mixture into thin films. We employed AuNCs as the plasmonic nanostructures owing to their tunable LSPR in the near-infrared (NIR) region and their remarkable photothermal effect.<sup>[6,13]</sup> When dispersed in a PVDF matrix, AuNCs could be used to generate localized heat in the PVDF film upon laser irradiation, leading to a ferroelectric–paraelectric phase transition in just a few seconds. This efficient plasmon-assisted phase transition allows us to pattern the ferroelectric  $\beta$  phase into an array of domains (or pixels) isolated by the paraelectric  $\alpha$  phase over a large area, enabling the facile fabrication of NIR-responsive pyroelectric devices.


Figure 1a shows a transmission electron microscopy (TEM) image of the AuNCs, which are characterized by a hollow interior and pores at the corners, together with an average outer edge length of about 48 nm and a wall thickness of approximately 6 nm. Homogeneous mixtures of AuNCs

[\*] J. Li, Dr. X. Yang, Dr. J. Xue, Dr. C. Zhu, Prof. Y. Xia  
The Wallace H. Coulter Department of Biomedical Engineering  
Georgia Institute of Technology and Emory University  
Atlanta, GA 30332 (USA)  
E-mail: younan.xia@bme.gatech.edu

M. Yang, Prof. Y. Xia  
School of Chemistry and Biochemistry  
Georgia Institute of Technology  
Atlanta, GA 30332 (USA)

X. Sun  
School of Materials Science and Engineering  
Georgia Institute of Technology  
Atlanta, GA 30332 (USA)

J. Li, Prof. H. Liu  
State Key Laboratory of Crystal Materials  
Shandong University  
Jinan, Shandong 250100 (P.R. China)

 Supporting information for this article can be found under:  
<http://dx.doi.org/10.1002/anie.201605405>.



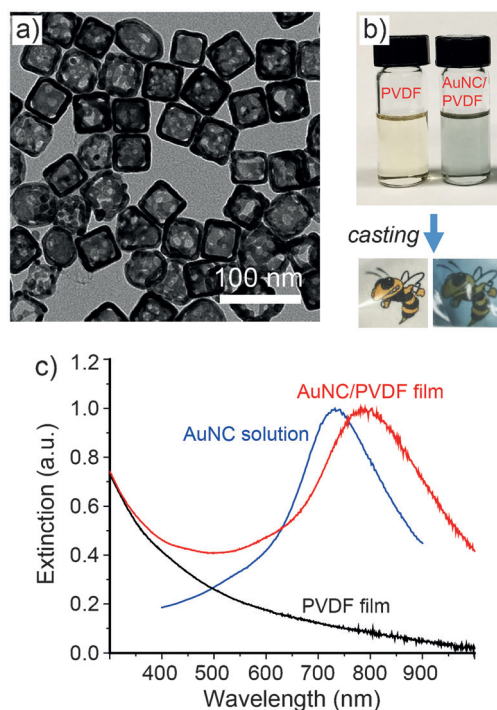


**Figure 1.** a) A typical TEM image of AuNCs. b) Photograph of a homogeneous mixture of AuNCs and PVDF obtained by mixing a suspension of AuNCs in ethanol with a PVDF solution in DMF. Transparent films were then cast from the mixture using a mold placed on a hot plate. c) Extinction spectra recorded for an ethanol suspension of AuNCs, PVDF film, and AuNC/PVDF film. The LSPR peak of the AuNCs was red-shifted from about 733 nm in ethanol to approximately 800 nm in PVDF.

and PVDF had a slightly blue color (Figure 1b), with no indication of aggregation. The as-obtained AuNC/PVDF composite films had a smooth surface (see the Supporting Information, Figure S1). The films were characterized by FTIR spectroscopy. As shown in Figure S2, the  $\beta$  phase<sup>[14]</sup> predominated the crystallization of PVDF during film casting, and the addition of AuNCs had essentially no effect on the formation of the  $\beta$  phase. The UV/Vis/NIR extinction spectrum (Figure 1c) recorded from the AuNC/PVDF film revealed a red shift of about 67 nm for the LSPR peak in comparison with that of AuNCs in ethanol suspension, which is due to the increase in the effective refractive index of the surrounding medium.<sup>[15]</sup> Herein, we purposely tuned the LSPR peak of the composite film to about 800 nm to overlap with the wavelengths of the lasers used in this work.

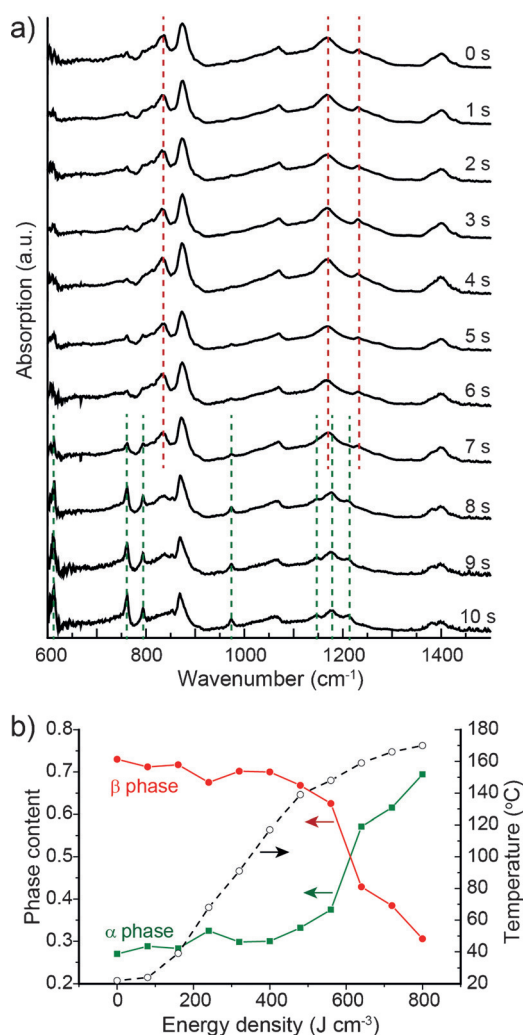
In an initial study, we investigated the plasmon-assisted heating process. The temperature of a AuNC/PVDF film upon irradiation with a 808 nm laser was monitored using a K-type thermocouple and an infrared camera. We also carried out measurements for pristine PVDF in addition to four composite films with different AuNC amounts (0.01, 0.02, 0.04, and 0.08 wt %). As shown in Figure S3, the temperature increased with both the mass ratio of the AuNCs and the laser power density. Within 20 s of irradiation, all of the AuNC/PVDF films showed a drastic increase in temperature, which was greater than in the case of the pristine PVDF film (see

Figure S4 for the IR images). When the laser power density was increased, the rise in temperature ( $\Delta T$ ) also increased accordingly for each composite film. We then quantitatively evaluated the ability of the composite films to convert light into heat by calculating the energy conversion efficiency ( $\eta$ ; see the Supporting Information). Furthermore, the AuNC/PVDF films exhibited good durability under long-term laser irradiation. As shown in Figure S5, the photothermal conversion efficiency of the composite films had not changed after five rounds of irradiation, whereas a reduction in temperature rise was clearly observed for a reference sample containing indocyanine green rather than the AuNCs. The much higher stability of the AuNCs over organic dyes would ensure the long lifetime of the devices.

We then studied the phase transition during the plasmon-assisted heating process. We observed that exposure to a 808 nm laser at  $1 \text{ W cm}^{-2}$  for less than 10 s was sufficient to induce the transition from the ferroelectric  $\beta$  phase to the paraelectric  $\alpha$  phase owing to the high photothermal conversion efficiency of the AuNCs. The formation of the  $\alpha$  phase in the composite film was confirmed by the time-elapsing FTIR spectra shown in Figure 2a. The peaks at 610, 765, 796, 973, 1144, 1167, and  $1211 \text{ cm}^{-1}$  for the  $\alpha$  phase were clearly visible while the peaks at 839, 1176, and  $1232 \text{ cm}^{-1}$  for the  $\beta$  phase disappeared. The thermally induced ferroelectric to paraelectric phase transition of PVDF has been reported to occur near its melting point (ca.  $170^\circ\text{C}$ ) through an intermediate amorphous or liquid-crystalline phase.<sup>[11a]</sup> When the laser energy added into the AuNC/PVDF film reached  $800 \text{ J cm}^{-2}$ , the corresponding temperature could be over  $170^\circ\text{C}$  (see Figure 2b). As such, the  $\beta$  phase crystal could melt to form an amorphous phase or a liquid-crystalline phase, followed by recrystallization into the  $\alpha$  phase. We calculated the  $\alpha$  and  $\beta$  phase content in the laser-irradiated region from the absorbance of the respective vibrational bands at  $765 \text{ cm}^{-1}$  for the  $\alpha$  phase and  $839 \text{ cm}^{-1}$  for the  $\beta$  phase. Upon irradiation for a short period of only 10 s, a AuNC/PVDF film with a dominating  $\beta$  phase (ca. 73 %) had been transformed into an  $\alpha$  phase dominated (ca. 70 %) film.

The efficient plasmon-assisted phase transition could also be employed for the fabrication of micropatterned ferroelectric domains. We could simply use a laser beam as a writing pen to create a patterned array of the  $\beta$  phase PVDF isolated by the nonpolar  $\alpha$  phase over a large area. To obtain a micropatterned ferroelectric thin film, a continuous laser beam was utilized to irradiate the AuNC/PVDF film on a motorized  $x, y$  stage (Figure 3a). The use of a 785 nm laser with a power of 25 mW and a stage moving speed of  $20 \mu\text{m s}^{-1}$  successfully produced micropatterned  $\beta$ -phase domains in the composite film. The phase contents of the irradiated and non-irradiated regions were visualized by Raman spectroscopy as shown in Figure 3b. The representative absorption peaks of 839 and  $796 \text{ cm}^{-1}$  for the  $\beta$  and  $\alpha$  phases, respectively, were selected, and the integrated intensities for each peak were mapped (Figure 3c,d). The pattern clearly shows a transition from the  $\beta$  phase to the  $\alpha$  phase in the laser beam path. The percentages of the  $\alpha$  and  $\beta$  phases were calculated and plotted in Figure 3e. The line profile clearly shows the patterned distribution of the  $\beta$  phase, with a minimum feature size of





**Figure 2.** a) FTIR spectra recorded for a AuNC/PVDF film upon irradiation with a 808 nm laser for different periods of time at  $1 \text{ W cm}^{-2}$ . b) Dependence of the phase content and the temperature change on the laser power density.

around  $20 \mu\text{m}$ . It is noteworthy that there was a transition gap of about  $10 \mu\text{m}$  between the  $\alpha$  and  $\beta$  phase dominated regions, which is mainly due to lateral thermal diffusion.

One of the major applications of the ferroelectric PVDF film is the detection of infrared signals. Conventionally, infrared sensors comprise a PVDF film sandwiched between two electrodes, with the top electrode serving as an absorption layer to pass the heat to the pyroelectric film.<sup>[16]</sup> This design may lead to heat loss and hinder the pyroelectric response of the detector. In our system, the pyroelectric film itself serves as the adsorption layer owing to the incorporation of AuNCs. When the AuNC/PVDF film is exposed to NIR irradiation, heat will be generated directly in the film owing to the photothermal effect, and the level of polarization in the film will then change as a result of the change in temperature. Therefore, when the level of polarization decreases upon heating under open-circuit conditions, the released surface charges will create a potential difference across the polar axis, similar to a charged parallel-plate capacitor.<sup>[17]</sup> For a parallel

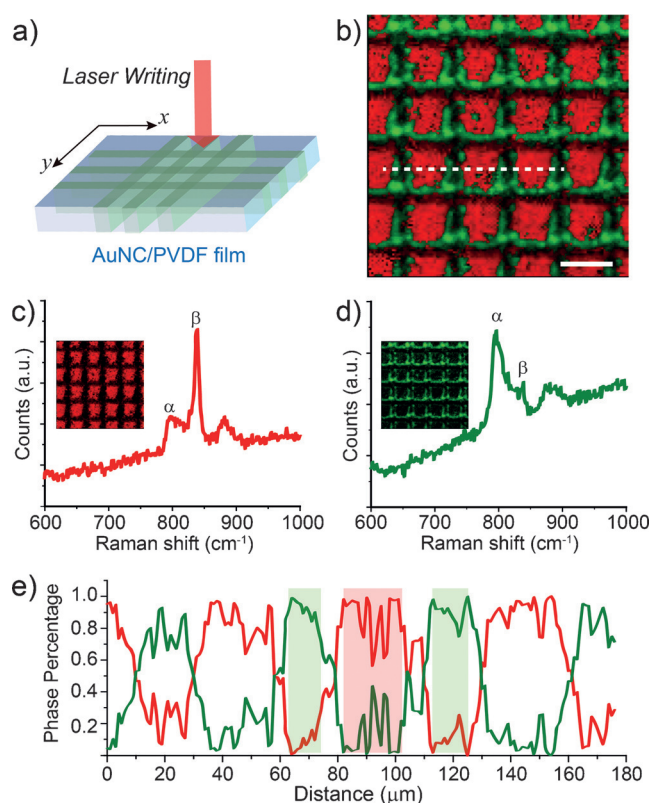


**Figure 3.** a) Phase patterning in a AuNC/PVDF film by direct laser writing. The 785 nm laser source of a Raman microscope was used, and the motion of the sample was driven by a software-controlled motorized stage installed in the microscope. b) Raman mapping of a AuNC/PVDF film over an area of  $250 \times 250 \mu\text{m}^2$ , exhibiting a patterned  $\beta$  phase distribution. Scale bar:  $50 \mu\text{m}$ . Representative Raman spectra of c) the non-irradiated regions ( $\beta$  phase dominating) and d) the laser-irradiated regions ( $\alpha$  phase dominating) in AuNC/PVDF. e) Profile of the phase content for the dashed line indicated in (b).

capacitor with a homogeneous electric field, the open circuit voltage  $V$  can be expressed as:

$$V = \frac{p}{\epsilon_{33}} d \Delta T$$

where  $p$  is the pyroelectric coefficient,  $\epsilon_{33}$  is the relative permittivity of PVDF,  $d$  is the film thickness, and  $\Delta T$  is the temperature change. Therefore, one direct approach to increase the open-circuit voltage generated by a AuNC/PVDF film with a specific thickness is to increase  $\Delta T$ . At a given irradiation energy,  $\Delta T$  is determined by the photothermal conversion efficiency ( $\eta$ ) of the composite film. As such, we presume that an enhancement in pyroelectric response can be achieved for the AuNC/PVDF film by increasing the mass ratio of the AuNCs. To measure the pyroelectric response to NIR irradiation, PVDF films with different AuNC mass ratios were sandwiched between two electrodes, with the bottom electrode being a copper tape and the top electrode being a mesh of Ag nanowires (see Figure S6 for the characterization). As shown in Figure S7, a higher AuNC mass ratio indeed led to a larger temperature



change as well as a higher voltage. The 0.08% AuNC/PVDF film developed a voltage of about 20 mV, which represents an increase of about 570% compared to the ca. 3 mV for a pristine PVDF reference sample. The incorporation of AuNCs clearly greatly enhanced the pyroelectric response of a PVDF-based pyroelectric device to NIR light.

The plasmon-assisted micropatterning of the ferroelectric phase together with the enhanced pyroelectric response further encouraged us to fabricate a pixilated array for infrared imaging. In a proof-of-concept study, we constructed a  $\beta$  phase sensing array with  $3 \times 3$  pixels as shown in Figure S8. The patterned copper layer served as both the mask for laser exposure and as the electrodes for measuring the electrical response (Figure 4a). The array was then selectively exposed to NIR radiation, and the open-circuit voltage from each pixel was recorded. The electric response of each pixel was then calculated and color-coded to show the difference. Figure 4b shows the illumination patterned to show the four letters T, E, C, and H. The illuminated pixels generated a signal of  $23 \pm 5$  mV. Negligible signals were detected from the blocked pixels, confirming that the pixels were isolated from each other by the  $\alpha$  phase barrier.

In conclusion, we have demonstrated the use of plasmonic nanostructures to induce a ferroelectric–paraelectric phase transition in a freestanding ferroelectric polymer film. The efficient plasmon-assisted phase transition could be conveniently combined with masked exposure for the fabrication of patterned ferroelectric domains or pixels. We also demonstrated the feasibility of constructing a pixilated ferroelectric phase pattern for infrared imaging. The simple and efficient method developed in this study is expected to promote both the low-cost fabrication and broader application of polymer-based flexible ferroelectronics.

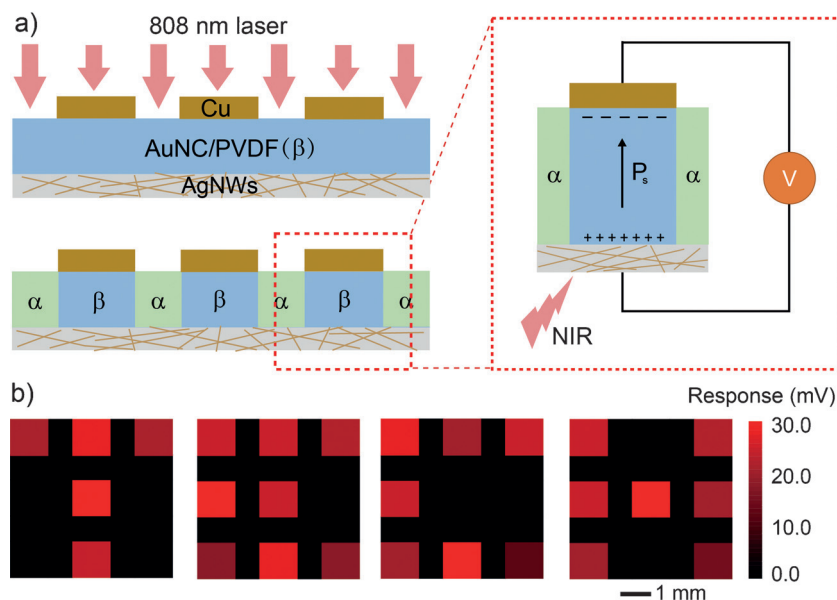


**Figure 4.** a) A proof-of-concept device for IR imaging with a phase-patterned AuNC/PVDF film by masking the laser irradiation with copper electrodes. b) The response of pixels in the sensing array to the incident irradiation, which was selectively blocked to form the four letters TECH.

## Acknowledgements

This work was supported in part by a grant from the NIH (R01, CA138527) and startup funds from Georgia Tech. As a jointly supervised Ph.D. student from Shandong University, J.L. was also partially supported by a fellowship from the China Scholarship Council.

**Keywords:** ferroelectricity · IR imaging · nanostructures · phase transition · surface plasmon resonance

**How to cite:** *Angew. Chem. Int. Ed.* **2016**, *55*, 13828–13832  
*Angew. Chem.* **2016**, *128*, 14032–14036

- [1] a) E. Ye, K. Y. Win, H. R. Tan, M. Lin, C. P. Teng, A. Mlayah, M.-Y. Han, *J. Am. Chem. Soc.* **2011**, *133*, 8506–8509; b) X. Huang, I. H. El-Sayed, W. Qian, M. A. El-Sayed, *J. Am. Chem. Soc.* **2006**, *128*, 2115–2120.
- [2] a) L. Tian, J. Luan, K.-K. Liu, Q. Jiang, S. Tadepalli, M. K. Gupta, R. R. Naik, S. Singamaneni, *Nano Lett.* **2016**, *16*, 609–616; b) M. S. Zielinski, J.-W. Choi, T. La Grange, M. Modestino, S. M. H. Hashemi, Y. Pu, S. Birkhold, J. A. Hubbell, D. Psaltis, *Nano Lett.* **2016**, *16*, 2159–2167.
- [3] a) J. Zeng, D. Goldfeld, Y. Xia, *Angew. Chem. Int. Ed.* **2013**, *52*, 4169–4173; *Angew. Chem.* **2013**, *125*, 4263–4267; b) G. L. Liu, J. Kim, Y. Lu, L. P. Lee, *Nat. Mater.* **2006**, *5*, 27–32.
- [4] a) S. Linic, U. Aslam, C. Boerigter, M. Morabito, *Nat. Mater.* **2015**, *14*, 567–576; b) M. L. Brongersma, N. J. Halas, P. Nordlander, *Nat. Nanotechnol.* **2015**, *10*, 25–34.
- [5] S. C. Nguyen, Q. Zhang, K. Manthiram, X. Ye, J. P. Lomont, C. B. Harris, H. Weller, A. P. Alivisatos, *ACS Nano* **2016**, *10*, 2144–2151.
- [6] M. S. Yavuz, Y. Cheng, J. Chen, C. M. Cobley, Q. Zhang, M. Rycenga, J. Xie, C. Kim, K. H. Song, A. G. Schwartz, *Nat. Mater.* **2009**, *8*, 935–939.
- [7] G. D. Moon, S.-W. Choi, X. Cai, W. Li, E. C. Cho, U. Jeong, L. V. Wang, Y. Xia, *J. Am. Chem. Soc.* **2011**, *133*, 4762–4765.
- [8] R. Hasegawa, Y. Takahashi, Y. Chatani, H. Tadokoro, *Polym. J.* **1972**, *3*, 600–610.
- [9] H. M. Manohara, E. Morikawa, J. Choi, P. T. Sprunger, *J. Microelectromech. Syst.* **1999**, *8*, 417–422.
- [10] a) S. J. Kang, Y. J. Park, J. Y. Hwang, H. J. Jeong, J. S. Lee, K. J. Kim, H. C. Kim, J. Huh, C. Park, *Adv. Mater.* **2007**, *19*, 581–586; b) Y. Liu, D. N. Weiss, J. Li, *ACS Nano* **2010**, *4*, 83–90.
- [11] a) P. J. Ratri, K. Tashiro, *Polym. J.* **2013**, *45*, 1107–1114; b) A. J. Lovinger, D. D. Davis, R. E. Cais, J. M. Kometani, *Macromolecules* **1986**, *19*, 1491–1494.
- [12] M. Wegener, J. Hesse, T. Wegener, R. Gerhard-Multhaupt, *J. Appl. Phys.* **2002**, *91*, 3193–3196.
- [13] a) S. E. Skrabalak, J. Chen, Y. Sun, X. Lu, L. Au, C. M. Cobley, Y. Xia, *Acc. Chem. Res.* **2008**, *41*, 1587–1595; b) J. Chen, C. Glaus, R. Laforest, Q. Zhang, M. Yang, M. Gidding, M. J. Welch, Y. Xia, *Small* **2010**, *6*, 811–817.
- [14] a) T. Boccaccio, A. Bottino, G. Capannelli, P. Piaggio, *J. Membr. Sci.* **2002**, *210*, 315–329; b) B. Luo, X. Wang, Y.



- Wang, L. Li, *J. Mater. Chem. A* **2014**, 2, 510–519.
- [15] M. A. Mahmoud, M. A. El-Sayed, *J. Am. Chem. Soc.* **2010**, 132, 12704–12710.
- [16] a) A. Armitage, K. Benjamin, D. Setiadi, H. Weller, T. Binnie in *Proc. of the Eighth Conference on Sensors and Their Applications, Glasgow*, **1997**, pp. 297–302; b) E. S. Kulkarni, S. P. Heussler, A. V. Stier, I. Martin-Fernandez, H. Andersen, C.-T. Toh, B. Özyilmaz, *Adv. Opt. Mater.* **2015**, 3, 34–38.
- [17] D. Zabek, J. Taylor, E. L. Boulbar, C. R. Bowen, *Adv. Energy Mater.* **2015**, 5, 1401891.

Received: June 2, 2016  
Published online: July 26, 2016